Iterative evaluation of the effect of long-range potentials on the solution of the Schrödinger equation

George Rawitscher
Department of Physics, University of Connecticut, Storrs, Connecticut 06268, USA
(Received 15 October 2012; revised manuscript received 24 January 2013; published 18 March 2013)

There are cases where the potentials present in the Schrödinger equation are of long range and have measurable effects as, for instance, for the interaction between atoms at low temperatures or for the calculation of atomic three-body collisions. In these cases, the solution of the Schrödinger equation for the wave functions by finite-difference or finite-element techniques may not achieve the desired accuracy. An iterative method is presented, based on the Lippmann-Schwinger integral equation, that is similar in spirit to the Born approximation but is applied only in the region of the potential tails. This procedure extends the numerical solution obtained for short distances to large distances without loss of accuracy. Numerical examples are presented for atomic van der Waals potentials C_n/r^n. For C_6/r^6, the size of the radial interval, for which an accuracy of 10^{-10} is achieved, is $\simeq$[100,1000] atomic units a_0. For the case of C_3/r^3, the required interval for the same level of accuracy is [4000,50 000], which, because of its large size, has to be subdivided into smaller partitions. The wave numbers k chosen for these examples correspond to atomic collision energies in the micro-Kelvin range. The larger the wave number k, the faster the rate of the convergence, and the limit $k \to 0$ is also investigated. A criterion is given for determining whether the iterations converge in that limit.

DOI: 10.1103/PhysRevA.87.032708 PACS number(s): 34.50.Cx, 31.15.xp

I. INTRODUCTION

At low temperatures, many of the atomic physics investigations require the solution of differential equations out to large distances. The recombination of three atoms requires a calculation out to a distance of 10^4 atomic units [1]. The magnetic dipole interaction between molecules involves coupling potentials that decrease slowly with distance as $1/r^3$ and require calculations out to long distances [2]. The occurrence of resonances in a diatomic system that includes dipole-dipole interactions also requires calculations out to large distances [3] because the interaction potential decreases like $1/r^3$. The calculations of Ref. [3] are based on a collocation method at Gaussian support points, that was introduced in 1973 [4]. The conventional finite-difference methods for solving the Schrödinger equation out to the large distances required here are not able to provide the necessary accuracy as shown in the Appendix.

The purpose of this paper is to describe a method that solves the Schrödinger equation out to large distances R_∞ iteratively, avoiding the loss of accuracy that occurs for such large distances with the conventional finite-element or finite-difference methods. The present method calculates two independent solutions Y and Z of the Schrödinger equation in the presence of the potential V_A but only in a restricted radial domain $[R_M, R_\infty]$. Here, V_A is the difference between the total potential and the sum of a Coulomb potential and a centripetal potential. The domain $[R_M, R_\infty]$ is chosen such that V_A in this domain is sufficiently small in order for the iterations to converge, R_M is such that the conventional numerical solution ψ_c of the Schrödinger equation in the domain $[0, R_M]$ is still sufficiently accurate, and R_∞ is chosen to be so large that the magnitude of V_A for $r \geqslant R_\infty$ is sufficiently small in order to obtain the desired accuracy. By matching ψ_c to Y and Z at R_M, the loss of accuracy described above can be mitigated substantially as will be illustrated by means of a numerical example. The iterative method to obtain Y and Z is based on the equivalent Lippmann-Schwinger integral equation, similar to what is performed in the conventional Born approximation [5]. The method is quite general and consists of performing integrals over only known functions, i.e., for each iteration, it does not solve an equation or diagonalize any Hamiltonian. This method, carried out in configuration space, can be extended to the solution of coupled-channel equations.

A method similar in spirit to the one presented here has been developed in the 1970s by Knirk [6]. It also is based on the Lippmann-Schwinger integral equation and iteratively propagates the solution from R_M to R_∞ by a matrix technique. However, in the numerical examples, only one iteration has been performed, attaining an accuracy of four significant figures. Iterative calculations in density-functional theory with special consideration of long-range effects have also been performed [7], a low-energy expansion of the Jost function for long-range potentials [8] has been given, and an effective potential has been developed [9] that incorporates the effect of long-range potentials. An adaptation of the quantum defect theory to a multichannel system has been developed [10], that approximates the long-range part of the calculation by Milne's phase-amplitude method [11]. However, the simplicity of the present method appears not to have been achieved previously.

II. NOTATION AND FORMALISM

For each partial wave, the total potential V includes the centripetal and Coulomb potentials,

$$V(r) = V_A(r) + \frac{L(L+1)}{r^2} + V_C, \tag{1}$$

where V_A describes the atomic or nuclear interaction between the colliding particles and V_C is the Coulomb potential, if present. The equation for the partial-wave radial function $\psi(r)$ to be solved is

$$\left(\frac{d^2}{dr^2} - \frac{L(L+1)}{r^2} - V_C + k^2\right)\psi(r) = V_A(r)\psi(r). \tag{2}$$

The wave number k is in units of a_0^{-1}, and the potentials are in units of a_0^{-2}, where a_0 is the Bohr radius and where the quantities in energy units are transformed to inverse length units by multiplication by the well-known factor $2\mu/\hbar^2$. The solutions $\psi(r)$ are normalized such that, asymptotically, they approach

$$\psi(r) \to F(r) + SH(r), \quad r \geqslant R_\infty, \tag{3}$$

where F and H are two linearly independent solutions of Eq. (2) for $V_A = 0$. As is well known, F describes the incident wave, H describes the scattered outgoing wave [12], and S is a constant that defines the scattering phase shift.

The un-normalized numerical solution of Eq. (2) in the domain $[0, R_M]$ is denoted as ψ_c (c for "computational"). If V_A is already negligible for $r \geqslant R_M$, then $R_\infty = R_M$, and by matching ψ_c to F and H at $r = R_M$ by the usual Wronskian procedure, one obtains the coefficients α and β,

$$\psi_c(r) = \alpha F(r) + \beta H(r), \quad r = R_M. \tag{4}$$

Once the constant α is obtained, the renormalized wave function (3) is given by $\psi(r) = \psi_c(r)/\alpha$ and $S = \beta/\alpha$. However, in the case that V_A has such a long range that the accuracy of ψ_c at R_∞ is unacceptable, then the method described below is preferable. This method consists of defining two new independent functions Y and Z that obey Eq. (2) in the domain $[R_M, R_\infty]$. Because Y and Z also obey the Lippmann-Schwinger integral equations,

$$Y(r) = F(r) + \int_{R_M}^{R_\infty} \mathcal{G}(r,r')V_A(r')Y(r')dr', \tag{5}$$

and

$$Z(r) = H(r) + \int_{R_M}^{R_\infty} \mathcal{G}(r,r')V_A(r')Z(r')dr', \tag{6}$$

the functions Y and Z also have well-defined boundary conditions, determined by the nature of the Green's function $\mathcal{G}(r,r')$. For the present application,

$$\mathcal{G}(r,r') = -\frac{1}{k}F(r_<)H(r_>), \tag{7}$$

where F and H are either spherical Bessel or Coulomb functions defined for a particular angular momentum number L as described, for example, in Refs. [12,13].

Explicit forms of Eqs. (5) and (6) are

$$Y(r) = F - \frac{1}{k}F(r)\int_r^{R_\infty} H(r')V_A(r')Y(r')dr' - \frac{1}{k}H(r) \times \int_{R_M}^{r} F(r')V_A(r')Y(r')dr', \tag{8}$$

and

$$Z(r) = H - \frac{1}{k}F(r)\int_r^{R_\infty} H(r')V_A(r')Z(r')dr' - \frac{1}{k}H(r) \times \int_{R_M}^{r} F(r')V_A(r')Z(r')dr'. \tag{9}$$

As a result of Eqs. (8) and (9), the values of Y and Z at $r = R_\infty$ are

$$Y(R_\infty) = F(R_\infty) + AH(R_\infty), \tag{10}$$

$$Z(R_\infty) = (1 + B)H(R_\infty), \tag{11}$$

where

$$A = -\frac{1}{k}\int_{R_M}^{R_\infty} F(r')V_A(r')Y(r')dr', \tag{12}$$

$$B = -\frac{1}{k}\int_{R_M}^{R_\infty} F(r')V_A(r')Z(r')dr'. \tag{13}$$

In order to match the function ψ_c to Y and Z at R_M,

$$\psi_c(r) = \tilde{a}Y(r) + \tilde{b}Z(r), \quad r \geqslant R_M, \tag{14}$$

one requires the values and the derivatives of Y and Z at $r = R_M$. They are given by

$$Y(R_M) = (1 + C)F(R_M), \tag{15}$$

$$Z(R_M) = H(R_M) + DF(R_M), \tag{16}$$

with

$$C = -(1/k)\int_{R_M}^{R_\infty} H(r')V(r')Y(r')dr', \tag{17}$$

$$D = -(1/k)\int_{R_M}^{R_\infty} H(r')V(r')Z(r')dr'. \tag{18}$$

The derivatives are given without loss of accuracy by $Y'(R_M) = (1 + C)F'(R_M)$ and $Z'(R_M) = H'(R_M) + DF'(R_M)$. In view of Eqs. (10) and (11), one has

$$\alpha = \tilde{a}, \tag{19}$$

and

$$\beta = \tilde{a}A + \tilde{b}(1 + B). \tag{20}$$

Since the asymptotic values of F and H at R_∞ are known, then, in view of Eqs. (3), (19), and (20), the value of ψ_c at R_∞ is also known. If V_A is negligible beyond R_∞, then A and B change only negligibly if R_∞ is made larger, and the scattering phase shift can be determined in terms of β/α, given by

$$S = A + \frac{\tilde{b}}{\tilde{a}}(1 + B). \tag{21}$$

This is the main result of the present section. In the section below, an iterative way of obtaining Y and Z is described.

III. THE ITERATION PROCEDURE

The iterative procedure for Y is as follows. One defines a correction $\chi^{(F)}$ to F,

$$Y(r) = F(r) + \chi^{(F)}(r), \quad r \geqslant R_M, \tag{22}$$

which, after some simple algebra based on Eq. (5), rigorously satisfies

$$\chi^{(F)}(r) = \int_{R_M}^{R_\infty} \mathcal{G}(r,r')V_A(r')[F(r') + \chi^{(F)}(r')]dr'. \tag{23}$$

Since both V_A and $\chi^{(F)}$ are small, the term $\chi^{(F)}(r')$ in the square brackets can be neglected, and one obtains the first-order approximation to $\chi^{(F)}$,

$$\chi_1^{(F)} = \int_{R_M}^{R_\infty} \mathcal{G}(r,r')V_A(r')F(r')dr'. \tag{24}$$

By defining the successive approximations to $\chi^{(F)}$ as

$$\chi^{(F)} = \chi_1^{(F)} + \chi_2^{(F)} + \cdots, \quad R_M \leqslant r \leqslant R_\infty, \tag{25}$$

one obtains the recursive expressions,

$$\chi_{n+1}^{(F)}(r) = \int_{R_M}^{R_\infty} \mathcal{G}(r,r')V_A(r')\chi_n^{(F)}(r')dr', \quad n = 1,2,\ldots . \tag{26}$$

The final expression for $Y(r)$ is

$$Y(r) = F(r) + \chi_1^{(F)}(r) + \chi_2^{(F)}(r) + \cdots, \quad R_M \leqslant r \leqslant R_\infty, \tag{27}$$

and the value of $Y(r)$ at $r = R_\infty$ is

$$Y(R_\infty) = F(R_\infty) + H(R_\infty)\sum_{n=1}^{\infty} A_n, \tag{28}$$

with

$$A_n = -\frac{1}{k}\int_{R_M}^{R_\infty} F(r')V_A(r')\chi_n^{(F)}(r')dr'. \tag{29}$$

For $Z(r)$, expressions similar to Eqs. (22)–(29) hold with F replaced by H,

$$Z(r) = H(r) + \chi_1^{(H)}(r) + \chi_2^{(H)}(r) + \cdots, \quad R_M \leqslant r \leqslant R_\infty. \tag{30}$$

The asymptotic value of $Z(R_\infty)$ is given by Eq. (11), with

$$B = \sum_{n=1}^{\infty} B_n, \tag{31}$$

where each value of B_n is given by

$$B_n = -\frac{1}{k}\int_{R_M}^{R_\infty} F(r')V(r')\chi_n^{(H)}(r')dr', \quad n = 1,2,\ldots . \tag{32}$$

The numerical examples presented in the next section examine the rate of convergence of the iterations and the high accuracy that can be obtained if the integrals are performed with high accuracy.

IV. NUMERICAL EXAMPLES

In these examples, the Coulomb potential is set to zero, $F = zj_L(z)$, and the function H is replaced by $G = -zy_L(z)$ so as to make all quantities real. Here, j_L and y_L are spherical Bessel functions, L is the angular momentum quantum number, and $z = kr$, k being the wave number. The potential V_A is equal to either V_3 or V_6, given by

$$V_3(r) = C_3/r^3 \quad \text{and} \quad V_6(r) = C_6/r^6, \tag{33}$$

where the distances r are in units of the Bohr radius a_0 and the C_i's are such that the potential V_i is in units of a_0^{-2} with $i = 3$ or 6. For the collision between two Rb or Sr atoms, whose atomic numbers are in the vicinity of 80 and using typical values of C_3 and C_6 of $\simeq -1$ and $\simeq -10^3$ in atomic energy units, respectively, after multiplication by the factor $2\mu/\hbar^2$, one obtains the following values of these coefficients in powers of a_0:

$$C_3 = -1.6 \times 10^5 a_0 \quad \text{and} \quad C_6 = -1.6 \times 10^8 a_0^4. \tag{34}$$

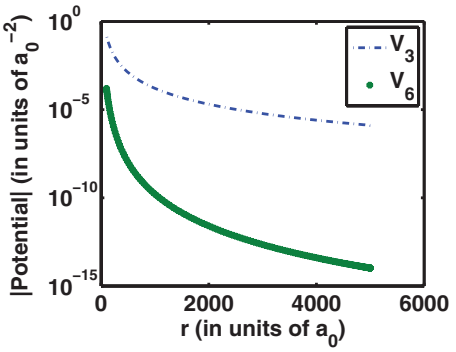

FIG. 1. (Color online) Absolute value of potentials V_3 and V_6, defined in Eqs. (33) and (34).

The absolute values of these potentials are illustrated in Fig. 1. The convergence of the iterated values of Y to the "exact" value of Y is expressed in terms of the error $\Delta Y(n)$,

$$\Delta Y(n) = \left| F + \sum_{n'=1}^{n} \chi_{n'}^{F} - Y \right|. \tag{35}$$

The exact comparison functions Y and Z are obtained numerically by solving the integral equations (8) and (9) by means of the spectral Chebyshev expansion method [14], whose accuracy 10^{-11} has been tested previously. The quantities A_n are obtained by first calculating $\chi_n^{(F)}$ by means of (26) and then evaluating the integrals (29). By substituting F by G, one obtains the corresponding results for B_n. The integrals are performed with a Gauss-Chebyshev method, described in Ref. [15], that uses the spectral integral equation method [14] and is accurate to $1{:}10^{-11}$. The iterations lead to powers of the integral,

$$I_1 = \int_{R_M}^{R_\infty} r\,V_A(r)dr, \tag{36}$$

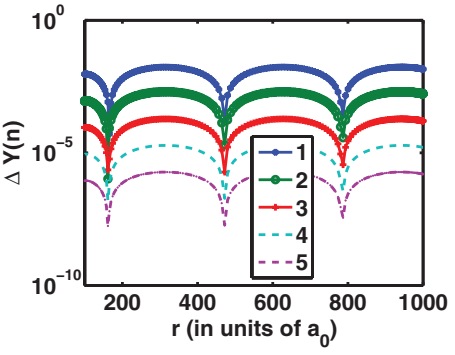

FIG. 2. (Color online) The error of the function Y after n iterations. The value of n is given in the legend, the potential is V_6, the wave number is $k = 0.01a_0^{-1}$, the angular momentum number is $L = 0$, and the radial partition is $100 \leqslant r \leqslant 1000a_0$.

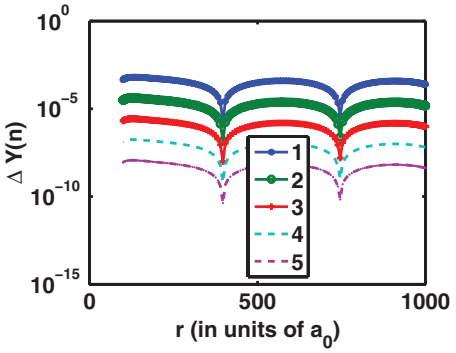

FIG. 3. (Color online) The same as Fig. 2 with $L = 2$.

and

$$I_2 = k \int_{R_M}^{R_\infty} r^2 V_A(r) dr. \tag{37}$$

If these integrals are finite and less than unity, then the iterations converge. This condition can be achieved if either the magnitude of the potential is sufficiently small in the range $[R_M, R_\infty]$ or if the range itself is sufficiently small as is discussed further below.

A. For the potential C_6/r^6

This potential is denoted as V_6 with the value of C_6 given by Eq. (34). The chosen radial interval is $[R_M, R_\infty] = [100, 1000]a_0$, and the values of L are 0 and 2. Since, at $R_\infty = 1000a_0$, the value is $V_6 \simeq 10^{-10}a_0^{-2}$, it is expected that the absolute error of the final phase shift is not larger than 10^{-10}. The convergence of the iterations to the functions Y for $L = 0$ and $L = 2$ with $k = 0.01a_0^{-1}$, according to Eq. (35), is displayed in Figs. 2 and 3, respectively. The results for the function Z are similar but are not shown. The convergence of $Y(n)$ and $Z(n)$ to Y and Z can also be seen by the convergence of the coefficients A_n and B_n. This convergence for various values of k is displayed Figs. 4 and 5, respectively.

These figures show that, for the smaller values of k, the convergence of the iterations gets progressively slower but reaches a stable value in the limit of $k \to 0$. An important consequence is that the long-range scheme described above

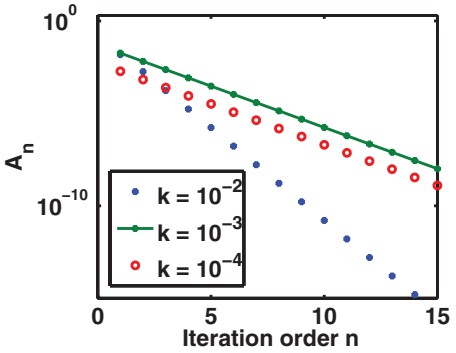

FIG. 4. (Color online) The convergence of the coefficients A_n with iteration n for various values of the wave number k expressed in units of a_0^{-1}. The potential is V_6, $L = 0$, and the radial partition is $[100, 1000]a_0$.

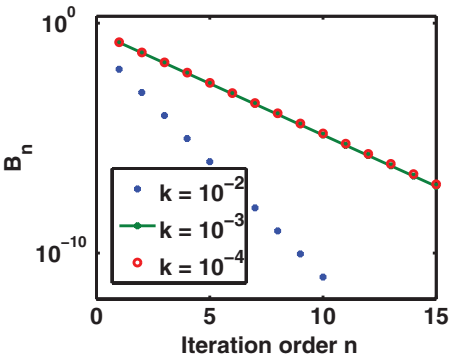

FIG. 5. (Color online) The same as Fig. 4 for the coefficients B_n.

can be applied to atomic physics conditions at ultralow temperatures.

B. For the potential C_3/r^3

This potential is much larger than V_6, and hence, the value of R_M also has to be much larger. For $r = 30\,000a_0$, the value of V_3 is $10^{-8}a_0^{-2}$, and hence, if the phase shift is to be accurate to 10^{-8}, the value of R_∞ should be $\geqslant 30\,000a_0$. If R_M is $\simeq 1000a_0$, the iterations in the full interval $[R_M, R_\infty]$ do not converge since $V_3(R_M) \simeq 10^{-4}a_0^{-2}$ is too large. Hence, it will be necessary to subdivide this interval into smaller partitions $[a,b]$, and the results from one partition will be matched to the results from the previous partition. The functions Y and Z in each partition are obtained iteratively by using the method described above with R_M and R_∞ replaced by a and b, respectively. The convergence properties of the iterations in partitions $[a,b]$ will be investigated next as follows.

If the size of a subpartition is δ, then $b = a + \delta$. For each chosen value of δ and a given value of k, the corresponding value of a is searched numerically so that after 19 iterations, $A_{19} < 10^{-8}$. The results are shown in Fig. 6. This figure shows that, for a large partition size δ (say 500) and a small value of k (say 10^{-5}), the value of a has to be large (about 15 000). If k increases, the corresponding value of a decreases because the rate of convergence increases. An additional analysis of the convergence results described above can be performed by

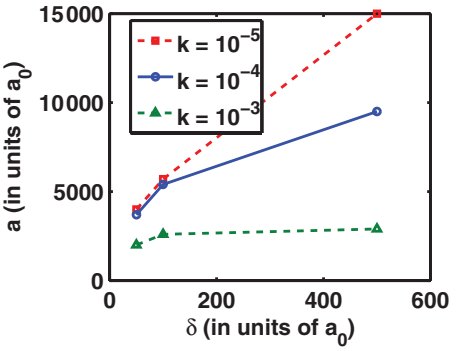

FIG. 6. (Color online) The value a on the left-hand side of the interval $[a, a + \delta]$ as a function of the size δ of this interval. The values of a are determined such that the convergence of the values of A_n reaches an accuracy of $< 10^{-8}$ after 19 iterations. The potential is V_3, and the values of k (in units of a_0^{-1}) are indicated in the legend.

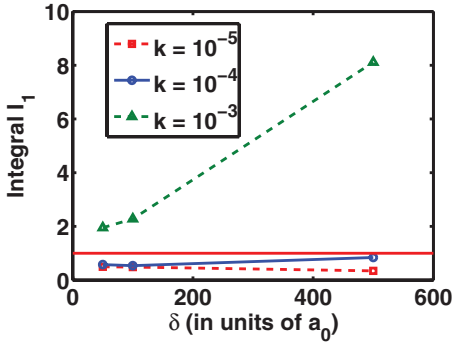

FIG. 7. (Color online) The integral $I_1 = \int_a^b r V_A(r) dr$ with $b = a + \delta$ as a function of δ and the wave number k, the latter given in units of a_0^{-1}. For a given value of δ and k, the corresponding value of a is determined numerically such that the iterations converge, which is the case for all the values of I_1 illustrated here. The values of a are illustrated in Fig. 6.

inspecting the values of the integral I_1, given by Eq. (36) and illustrated in Fig. 7. The figure shows that, when $|I_1| < 1$, the iterations converge even for the smallest values of k. For larger values of k, the convergence improves, and I_1 can be larger than unity.

The results in this section show that, for a V_3 potential, the iterative method described here is not as as useful as for the V_6 case for ultracold collisions.

V. SUMMARY AND CONCLUSIONS

An iterative method is developed to calculate scattering solutions of the Schrödinger equation, whose potential V_A is of very long range. Here, V_A is the difference between the total potential V and the sum of the centripetal and Coulomb potentials. In the radial domain where the long-range part of the potential V_A is small, two independent solutions of the Schrödinger equation are obtained by an iterative method. By matching the solution calculated in the short-range radial domain to the ones obtained for the long-range domain, it is possible to have the final solution obey the appropriate asymptotic boundary conditions and to determine the scattering phase shift. The purpose of this method is to avoid the large numerical errors that can occur when propagating the solution to large distances by conventional finite-difference or finite-element methods. The iterations are similar in spirit to the Born approximation since they are based on the Lippmann-Schwinger integral equation and they consist of integrals over known functions. The rate of convergence of the iterations depends on the size of the long-range part of the potential, on the size of the radial domain, and on the value of the wave number k. In the limit $k \to 0$, convergence still occurs, provided that the long-range part of the potential is sufficiently small such that the absolute value of the integral I_1, Eq. (36), is less than unity. A numerical example, involving potentials C_6/r^6 and C_3/r^3 for angular momentum number $L = 0$ and 2, is presented for a range of values of the wave number k that correspond to kinetic energies of the colliding atoms in the micro-Kelvin region. For the potential C_3/r^3, the rate of convergence of the iterations is not as favorable as that for the C_6/r^6 potential, and for this case, other methods, such as the phase-amplitude method [11], should be investigated. The present method can be generalized to include the case of coupled equations and is expected to be useful for investigating the collision of atoms at very low temperatures.

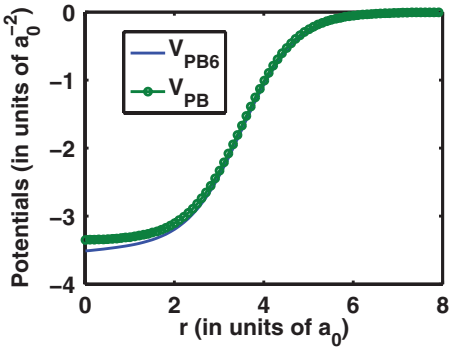

FIG. 8. (Color online) Potential V_{PB} is of a Woods-Saxon form that has no repulsive core at the origin and decays exponentially at large distances. To V_{PB}, the potential V_{PB6} has added a potential of the form $\bar{C}_6/r^6$, whose repulsive core has been smoothly suppressed.

ACKNOWLEDGMENTS

Conversations with Professor R. Coté and Dr. I. Simbotin are gratefully acknowledged.

APPENDIX

A numerical analysis of the accuracy of the finite-difference Numerov method is described here. It is shown that the accuracy decreases to unacceptable values in the regime of cold-atom collisions. Numerov's method is also denoted as Milne's corrector method and is given by Eq. 25.5.21 in Ref. [13]. In this method, the error of propagation of the wave function from two previous points to the next point is on the order of h^6, where h is the radial distance between the consecutive equispaced points.

The calculation is performed for the potential V_{PB6}. This potential consists of a conventional Woods-Saxon-type (without hard core) denoted as V_{PB}, Eq. (A1), to which is added a potential V_{R6}, Eq. (A2), that, at large distances, decreases with distance r proportional to r^{-6}. At short

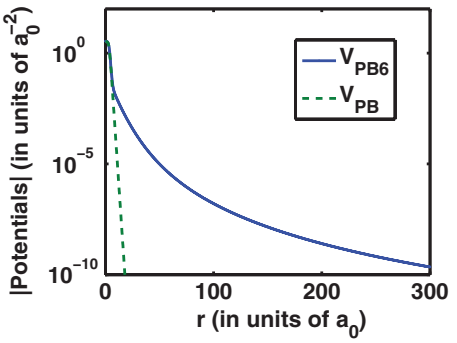

FIG. 9. (Color online) The absolute value of the potentials illustrated in Fig. 8.

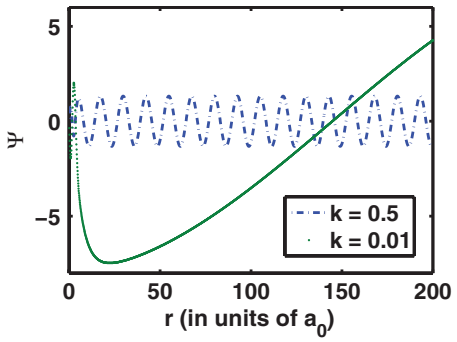

FIG. 10. (Color online) Wave functions corresponding to V_{PB6} as a function of radial distance, for two different values of the wave number k (in units of a_0^{-1}). For $k = 0.01$ the wave function reaches a maximum of about 8 at $r = 300a_0$, and goes through zero at $450a_0$. The reason for this large amplitude is because the phase shift is near the value $3\pi/2$, that occurs at $k = 0.015a_0^{-1}$.

distances, the singularity at the origin is smoothly eliminated by a radial mapping transformation Eq. (A3),

$$V_{PB}(r) = -3.36/[1 + \exp\{(r - 3.5)/0.6\}], \quad \text{(A1)}$$

$$V_{R6}(r) = -3.6458 \times 10^5/\mathcal{R}^6, \quad \text{(A2)}$$

$$\mathcal{R}(r) = r/[1 - \exp(-r/10)], \quad \text{(A3)}$$

$$V_{PB6} = V_{PB} + V_{R6}. \quad \text{(A4)}$$

The potentials are given by the equations above; the units of the constants are such that the potentials are in units of a_0^{-2} and the lengths are in units of a_0. The addition of V_{R6} to V_{PB} has a small effect near the origin as shown in Fig. 8, and the effect at large distances is illustrated in Fig. 9. The wave function in the presence of V_{PB6} is illustrated in Fig. 10 for two values of the wave number k. The value of $\tan(\delta)$ is obtained by obtaining the wave function by means of the Numerov method, normalizing it by matching it to F and G at $R_M = 200a_0$ and then evaluating the integral,

$$\tan(\delta) = -(1/k)\int_0^R \sin(kr)V_{PB6}\psi(r)dr. \quad \text{(A5)}$$

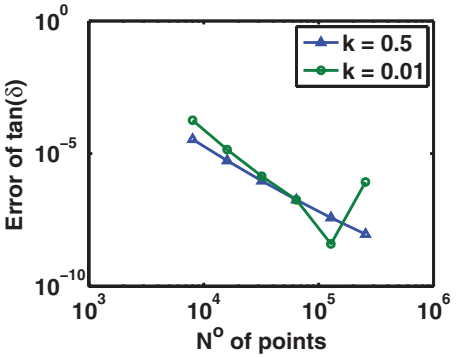

FIG. 11. (Color online) The accuracy of $\tan(\delta)$ as a function of the number of Numerov mesh points in the radial interval [0, 200] (in units of a_0) for two values of the wave number k (in units of a_0^{-1}).

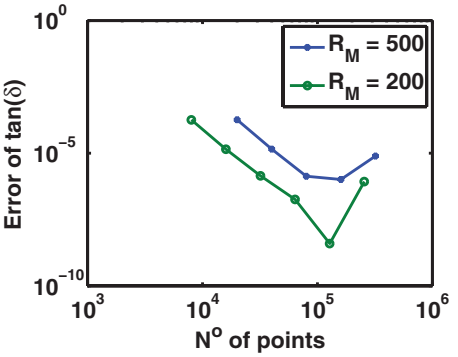

FIG. 12. (Color online) The accuracy of $\tan(\delta)$ as a function of the number of Numerov mesh points for two radial intervals $[0, R_M]$ (in units of a_0) for a wave number $k = 0.01a_0^{-1}$.

Use of this expression is preferable to using the result $\tan(\delta) = S = \beta/\alpha$ with β and α as defined in Eq. (4). The reason is that Eq. (A5) is more accurate because it suppresses the error of ψ for large distances where the potential is small. The error of $\tan(\delta)$ is obtained by comparing it to the result obtained by the spectral Chebyshev expansion method, which is accurate to $1{:}10^{-11}$, and the result is displayed in Fig. 11. This graph shows that the accuracy of $\tan(\delta)$ depends on the value of the wave number k. The accuracy decreases as k decreases, probably because, for the smaller k, the wave function has fewer oscillations, and the errors do not cancel as well as for a wave function with more oscillations.

For $k = 0.01a_0^{-1}$ and $R_M = 200a_0$, a maximum accuracy of 2×10^{-7} for $\tan(\delta)$ is obtained with 6×10^4 mesh points. For the larger value of $R_M = 500a_0$, the maximum accuracy deteriorates to 10^{-6} as shown in Fig. 12. The computational time is displayed in Fig. 13. The computation is performed on a desktop using an Intel TM2 Quad with a CPU Q 9950, a frequency of 2.83 GHz, and a random access memory of 8 GB. Maximum accuracy is obtained with approximately 10^5 mesh points for both values of R_M, whereas, for a larger number of mesh points, the accumulation of errors reduces the accuracy again. As can be seen from Fig. 13, the maximum accuracy with the Numerov method requires approximately 100 s of computing time as compared to

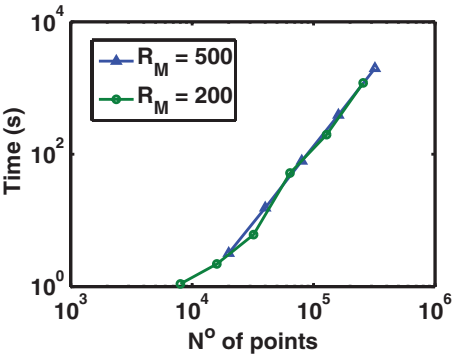

FIG. 13. (Color online) Computational time of $\tan(\delta)$ as a function of the number of mesh points in two radial intervals $[0, R_M]$ with R_M (in units of a_0) indicated.

0.8 s for the spectral Chebyshev method, whose accuracy is 10^{-10} or 10^{-11}. The computation time for the 19 iterations required for the each of the results displayed in Fig. 7 is 4 s, which amounts to 0.2 s per iteration. For these calculations, the number of Chebyshev support points for the whole radial interval is 200. A comparison of the Numerov method with a finite-element method, that is based on a discrete variable representation, was also performed in Ref. [16].

Figures 11–13 demonstrate that the deterioration in accuracy and the increase in computational time with increasing distance makes the Numerov method unsuitable for the long-range calculations required to describe the collision of atoms at low temperatures.

[1] B. D. Esry, C. H. Greene, and J. P. Burke, Jr., Phys. Rev. Lett. **83**, 1751 (1999).

[2] Z. Pavlovîć, R. V. Krems, R. Coté, and H. R. Sadeghpour, Phys. Rev. A **71**, 061402(R) (2005).

[3] Zhe-Yu Shi, Ran Qi, and Hui Zhai, Phys. Rev. A **85**, 020702(R) (2012); V. Roudnev and M. Cavagnero, J. Phys. B **42**, 044017 (2009).

[4] C. de Boor and B. Swartz, SIAM J. Numer. Anal. **10**, 582 (1973).

[5] A. Messiah, *Quantum Mechanics* (Wiley, New York, 1961), Eqs. (19.40) and (19.43).

[6] D. L. Knirk, J. Chem. Phys. **57**, 4782 (1972).

[7] E. Fromager and H. J. A. Jensen, J. Chem. Phys. **130**, 54112 (2009).

[8] K. Willner and F. A. Gianturco, Phys. Rev. A **74**, 052715 (2006).

[9] D. Masson and E. Prugovecĉki, J. Math. Phys. **17**, 297 (1976).

[10] J. P. Burke, Jr., C. H. Greene and J. L. Bohn, Phys. Rev. Lett. **81**, 3355 (1998).

[11] W. E. Milne, Phys. Rev. **35**, 863 (1930).

[12] R. H. Landau, *Quantum Mechanics II* (Wiley, New York, 1990).

[13] *Handbook of Mathematical Functions*, edited by M. Abramowitz and I. Stegun (Dover Publications Inc., New York, 1972).

[14] R. A. Gonzales, J. Eisert, I. Koltracht, M. Neumann, and G. Rawitscher, J. Comput. Phys. **134**, 134 (1997); R. A. Gonzales, S.-Y. Kang, I. Koltracht, and G. Rawitscher, *ibid.* **153**, 160 (1999); A. Deloff, Ann. Phys. (NY) **322**, 1373 (2007).

[15] G. Rawitscher and I. Koltracht, Computing Sci. Eng. **7**, 58 (2005); G. Rawitscher, in *Topics in Operator Theory*, Operator Theory: Advances and Applications, edited by T. Hempfling, Vol. 203 (Birkäuser Verlag, Basel, 2009), pp. 409–426.

[16] J. Power and G. Rawitscher, Phys. Rev. E **86**, 066707 (2012).